

PROCEEDINGS OF SPIE

[SPIDigitalLibrary.org/conference-proceedings-of-spie](https://spiedigitallibrary.org/conference-proceedings-of-spie)

Scatterometry and AFM measurement combination for area selective deposition process characterization

Mohamed Saib, Alain Moussa, Anne-Laure Charley,
Philippe Leray, Joey Hung, et al.

Mohamed Saib, Alain Moussa, Anne-Laure Charley, Philippe Leray, Joey Hung, Roy Koret, Igor Turovets, Avron Ger, Shaoren Deng, Andrea Illiberi, Jan Willem Maes, Gabriel Woodworth, Michael Strauss, "Scatterometry and AFM measurement combination for area selective deposition process characterization," Proc. SPIE 10959, Metrology, Inspection, and Process Control for Microlithography XXXIII, 109591N (26 March 2019); doi: 10.1117/12.2515177

SPIE.

Event: SPIE Advanced Lithography, 2019, San Jose, California, United States

Scatterometry and AFM measurement combination for Area Selective Deposition process characterization

Mohamed Saib^a, Alain Moussa^a, Anne-Laure Charley^a, Philippe Leray^a, Joey Hung^b, Roy Koret^b, Igor Turovets^b, Avron Ger^b, Shaoren Deng^c, Andrea Illiberi^c, Jan Willem Maes^c, Gabriel Woodworth^d AND Michael Strauss^d

^a imec, 3001 Leuven, Belgium

^b Nova Measuring Instruments, LTD, P.O. Box 266, Weizmann Science Park, Rehovot 76100, Israel

^c ASM Belgium, Kapeldreef 75, Leuven, Belgium

^d Thermo Fisher Scientific, 5350 NE Dawson Creek Drive, Hillsboro, OR 97124, USA

ABSTRACT

With the Area Selective Deposition (ASD) technique, the material is deposited on desired areas of the sample surface. The control of such process implies accurate characterization of the deposited material on both growth and non-growth surfaces. This requires, first a good measurement capability to quantify the geometry of the deposited layer, and second, a proper assessment of the process selectivity. In this work, we show how to combine two complementary measurement techniques to overcome their individual inherent limitations¹ for ASD applications. Scatterometry, the first measurement technique, has been applied to the characterization of the deposited layer geometry properties because of its high sensitivity to dimensional features and material. To complement the ASD performance characterization with the local information, Atomic Force Microscopy (AFM) has been used to access the topography details of the analyzed surfaces. We have analyzed the AFM images with the power spectral density (PSD) approach to identify undesired material deposition in the non-growth area and thus to characterize process selectivity through the comparison to a reference sample. Experimental validation of the scatterometry and AFM techniques for ASD applications has been done on wafers having various selectivity levels. The scatterometry metrology measured accurately the thickness of the deposited layer on both growth and non-growth areas when the deposited layer became uniform. The lateral overgrowth was quantified as well with the same technique and showed some changes from process condition to another. In addition, the PSD analysis applied to the AFM images was able to probe minutely the nanoparticles nucleation on the non-growth area and as result has revealed the selectivity transition regimes. Later, we have built a hybrid model by the combination of the 2 metrologies results and validated its predictions on test wafers.

Keywords: Scatterometry, AFM, Area-Selective Deposition, Power Spectral Density, Hybrid metrology, ALD

1. INTRODUCTION

The Integrated Circuits (IC) industry is always searching for solutions to build electronic devices with even higher performance. To that end, continuous manufacturing processes improvements are made by adjusting either the process parameters or sometimes by proposing new concepts. In the race for process optimization, the metrology plays a central role because it reveals the more important properties of shaped nanostructures. Over the last few years, the aggressive shrinking of critical dimensions has produced a constraint escalation on metrology, in particular, to provide high sensitivity to heterogeneous samples parameters. Many efforts are devoted to the resolution of metrology issues by combining or hybridization of multiple elementary metrology techniques^{2, 3, 4, 5}. This way to proceed is very promising for metrology since it allows capacities improvement at lower cost, simply by coupling the output of several measurement techniques. By this way, the weaknesses of each individual technique are compensated by the strengths of the rest of the metrology techniques and the picture provided by the combination on studied samples is completer and more reliable. Nonetheless, the crossing of measurements suggests defining how the measurement aggregation will be done. Usually, there are 2 main ways to combine the metrology results. In the first implementation, the metrology tools are classified in various importance ranks. The measurements data of each metrology rank are injected as an entry in the metrology tools with higher rank in order to consolidate their results. The final measurements are provided by the higher rank metrology. The cascading architecture aims progressively to make the results more and more reliable. This approach is often successfully used in scatterometry to mitigate the correlation problems between the parameters of the studied stacks where some features are measured on separate targets and injected in the global scatterometry model. In the second implementation of the metrology combination, there is no hierarchy between the measurement tools. The principle is that all measurements are describing with equivalent importance the characterized samples. We distinguish 2 cases during the experimental data fusion. The first case is perceptible when the competitor metrology techniques are providing equivalent parameters and the results are in contradictory like in the context of measurement of the CD (Critical Dimension) dimension by CDSEM tool and scatterometry. The user should define how the experimental data will be interpreted or mixed in such configurations. In the second case, the competitor metrology techniques are providing data describing heterogeneous properties of the studied sample as for instance the case of using the CDSEM for measuring the CD and the ellipsometry for measuring the thickness of layers. There is no conflict possible between the metrologies outcomes because the measurements cannot be in contradictory. Hence, we don't need any adjustment between the measurement results. In this work, we have used the last metrology combination architecture for the combination of the metrology results because the 2 metrology techniques are providing heterogeneous measurements.

The goal of this paper is to propose new metrology to analyze the performance of the Area Selective Deposition (ASD) process by combining 2 measurement techniques. We have chosen to setup a metrology for the characterization of this process technique because it gained importance in recent years for the manufacturing of multi-layer nanostructures. The ASD process belongs to the bottom-up approaches and was developed to overcome the limitations of the standard processes (top-down approaches) in term of layer-to-layer misalignment and etching damage on the stack. In addition, the conventional processes implementation is becoming as well very complex and very costly. The key aspect of the ASD process is that the deposited atoms are spontaneously self-aligned as wanted in the fabrication scheme, which means there is no need to have lithography and etch steps to pattern nanostructures as in the conventional process. The benefit being double, the alleviation of the manufacturing cost while removing overlay issues. In ASD, the layer deposition is constrained to precise areas of the target sample surface^{6, 7}. Usually, the deposition surface is already patterned and composed of 2 materials A and B which will define the areas where the material of interest (named C) will grow or not (figure 1). In practice, during the ASD process, either the surface A is activated to facilitate the atoms nucleation, or the surface B is inhibited to block their nucleation. In the principle, there is no difference between the two implementations since the nucleation on the surface A is preferred and prevented on the B surface. From a chemical point of view, the differentiation between the two sample surfaces occurs by exploiting the chemical bonds properties of the layers A and B. The completion of ASD requires to link locally to all surface atoms a molecule which allows or blocks its chemical reaction with the atoms of the material C. With each of both implementations, the nucleation of the material C atoms occurs exclusively on the top of surface A until the shape of a monolayer. The surface activation or inhibition cycle is repeated several times to maintain the sample surface properties on the initial configuration and thus pursue the layer growth until the patterned structure will be formed.

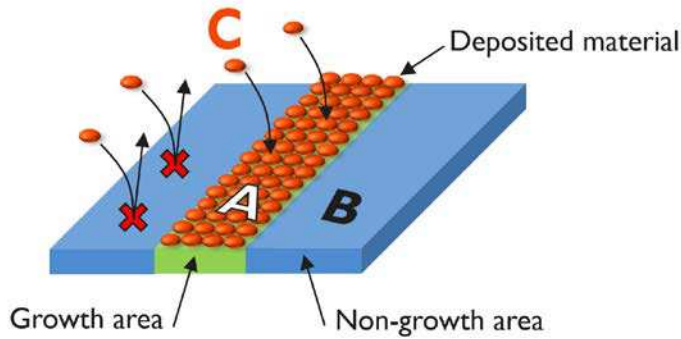
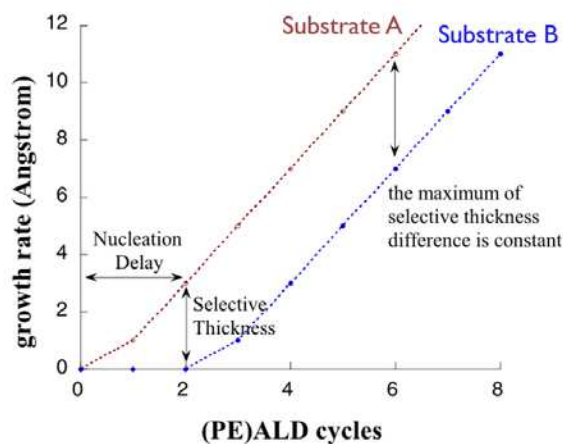
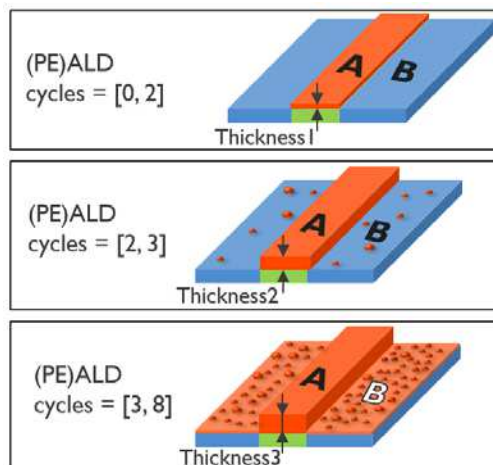


Figure 1: Illustration of the ASD process principle where the atoms of the material C nucleate exclusively on the growth area (surface A)

Theoretically, the nucleation process in ASD is fully controlled in order to keep the selectivity at its best. Nevertheless, experimental observations often reveal gradual degradation of the process selectivity caused most of the time by the cumulated defects on the top surface of the substrate B. To illustrate this, the figure 2⁸ represents a typical plot of the growth rate of the material C on sample having two surfaces A and B, as function of the atomic layer deposition cycles. The material C has similar growth on both substrates but with a delay for the substrate B, called nucleation delay. It results in various states of the sample geometry that could be depicted in 3 process phases. The first phase, with typically ALD cycles in the range [0, 2], the layer C grows exclusively on the surface A and the ASD behaves as an ideal selective process. Thereafter, we come to the second phase of the process which occurs for ALD cycles between 2 and 3. In this phase, the deposited layer on surface A pursues its linear growth but with some atoms of the material C which begins to nucleate above the surface B⁹. This is explained in the literature by the escalation of the number of surface defects. At this stage, the process has a low loss of selectivity. In the third and last phase, above 3 ALD cycles, the layer C grows in an identical way over both sample surfaces and without any selectivity. This process behavior should be avoided because it is in contradiction with the ASD purpose.



(a)



(b)

Figure 2: (a) Growth rate plot of the material C on the top of the substrates A and B, versus the number of ALD cycles in ASD process. (b) ASD stack examples got for (PE)ALD cycles [0, 2], [2, 3] and [3, 8]

We have identified in this study three geometrical properties that when measured simultaneously, give an exhaustive view of the ASD process quality (Figure 3). The first geometrical property is the deposited layer thickness measured separately above the two surfaces A and B and called Thk_A and Thk_B . By comparing the 2 thicknesses of layer C, three types of the process performance are distinguishable, that we will discuss below. The first case happens when the thicknesses Thk_A

and Thk_B are both at zero which means no layer is deposited yet. This indicates that we are at the beginning of the ASD process and at this stage, we cannot evaluate the process selectivity. The second case is when the 2 parameters Thk_A and Thk_B are non-zero, the ASD process is considered as having a bad selectivity because the material grows on both surfaces without distinction. In the third case, the Thk_A is non-zero and the Thk_B is zero. Further analysis are required to determine if the ASD process quality is good or intermediate.

To finalize the assessment of the process quality, we need further analysis. The second geometrical property designates the lateral overgrowth of the deposited layer, i.e. the overlap between the grown structure above the surface A and the adjacent surface B. For some applications, this overlap is prohibited because it affects the performance of the built nanostructures. The third and last property is the quantity of the nucleated atoms of material C above the surface B. With this property, even a very low change in selectivity will be detected since the layer growth arises initially from few nucleated atoms. Ultimately, fewer atoms are nucleated above B, better is the ASD selectivity.

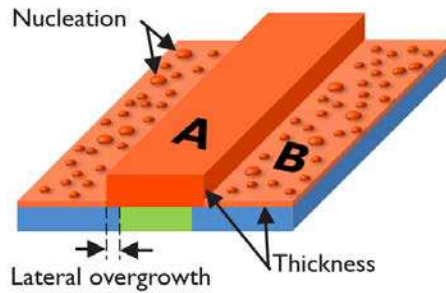


Figure 3: Geometrical properties to investigate in order to assess the selectivity of the studied ASD process

2. METROLOGY FOR ASD SAMPLES

Given there is no single metrology that could address the measurement of the 3 sample properties quoted above, we have decided in this work to combine two powerful complementary measurement techniques which are scatterometry and Atomic Force Microscopy (AFM).

2.1 Scatterometry:

Scatterometry is a model-based technique suitable for the characterization of the layer thicknesses deposited above the surfaces A and B and the lateral overgrowth because it has a high sensitivity to dimensional features and material. The scatterometry provides global information as it gives an averaged signal over the spot size. Basically, the scatterometry is an optical metrology technique (Figure 4), where the investigated sample surface is illuminated with a light beam having controlled polarization properties, usually linear. During the light scattering by patterns geometry, the optical polarization undergoes several changes proportional to various sample dimensions. Later, the scattered beam by the sample passes through an analyzer in order to isolate the phase changes of the light before its measurement with an optical sensor. The scatterometry is able to measure exclusively structures in a grating and with measurement area size larger than the source spot size. To extend the metrology efficiency, the Nova T600 scatterometry tool used in this work exploits a broad range of wavelengths (235 to 970nm), as well as multiple normal and azimuthal incidence angles. The set of measured spectra encodes the pattern profile properties in a complex manner, that eliminate any possibility of direct exploitation of scatterometry measurements by experiments. The exclusive practical solution is to build a parametrized optical model of the target structure and simulate the theoretical spectra by varying geometry parameters until it is matched with experimental measurements. This well-known mathematical processing is called inverse problem solution and achieved by using a library of pre-computed spectra to avoid the computation time-consuming. A single calibration allows extracting all structure dimensions at the same time. The scatterometry results require to be complemented by very local sample information about the nucleation state in the non-growth area.

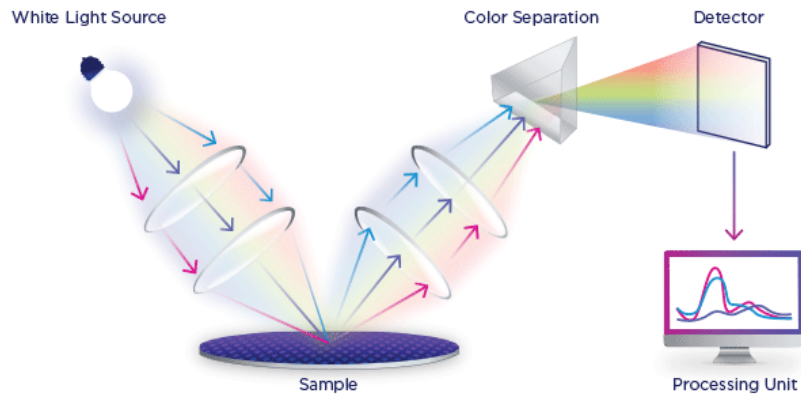


Figure 4: Illustration of the scatterometry set-up

2.2 Atomic Force Microscopy:

The second metrology used in this work is the nondestructive AFM technique from Park Systems. This metrology has large ability to characterize very tiny objects which makes it a good candidate to the characterization of the atom's nucleation in ASD samples. We have used the AFM tool in the mode true non-contact where the cantilever is put above the investigated sample and has on its extremity a very sharp tip. To optimize the measurement accuracy, we have used a cylindrical tip with high aspect ratio. During the measurement phase, the sample is moved in the XY plane to scan all its surface. The cantilever is oscillating at the resonance frequency and due to repulsion forces between the surface and the tip, the cantilever will bend more or less away from the sample. The position detector records the bending of the cantilever due to a laser beam that is reflected on the top of it. As the tip goes through the analyzed surface, the AFM collects gradually the topography data and delivers it as a map in a 3D image. Despite the AFM images contains all raw data relative to the surface under investigation, but they cannot be used immediately.

In this section, we will describe the algorithm that was developed in the frame of this work and allowing to quantify the nucleated atoms above the surface of interest. This approach is based on the interpreting the change in topography of the surface to investigate as a revelator of atoms nucleation. The basic principle of this technique is to consider the AFM image as ordinary fluctuating signal and to process it by using the Power Spectral Density (PSD) function^{8, 10, 11}. Basically, The PSD function oversimplifies the representation of fluctuating signal content, because it reveals its frequency dependence. Thereby, many significant properties of the signal are disclosed by both the shape and amplitude of the computed function. Mathematically, the PSD assessment is done in 2 steps. First, the raw signal is decomposed into elementary sine functions as described in the Fourier transform theory. Later on, the power of the signal is computed according to Parseval's theorem. The PSD curves show most of the signal properties. Indeed, the PSD curve can be split usually in 2 regimes, low and high frequency. In the low-frequency range, the PSD is almost flat wherein the high-frequency range it is decreasing gradually. In figure 5, we illustrate with an example the goal of use of the PSD function. Let's consider 2 random temporal signals A and B where the signal B is formed of signal A and a high frequency component. The PSD curves will be overlapped in the low frequency range because both signals have same low frequency signal components. In contrary to low frequency, in the high frequency range, the PSD of signal B will be upward shifted compared to one of signal A as a result of the additional signal component compared to signal A.

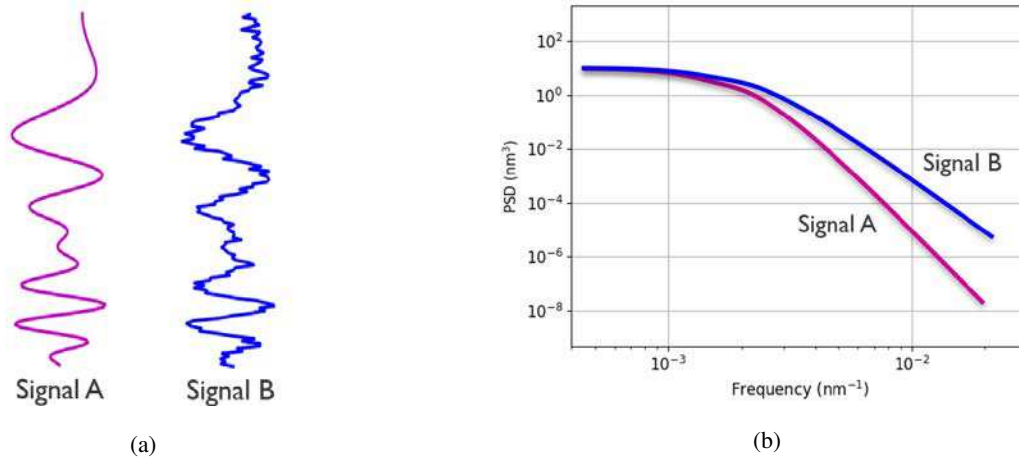


Figure 5: (a) 2 random temporal signals where the signal B is composed of signal A and a high frequency component. (b) 2 representative PSDs computed on signals A and B

In this work, atoms nucleation is revealed from the topography signal variation on a sample to study compared to a reference. The flowchart of the algorithm is shown in the figure 6 (a). We start the analysis of the AFM images by the localization of all similar sections over the sample surface, as for instance the center of the non-growth areas (trenches). Then, we extract their topography signal from AFM images and compute the PSD function on each of them. As the PSDs are extracted from comparable locations, their average will enhance the signal to noise ratio. At this stage, the total fluctuations of the AFM topography signal are caused by both the topography of the sample surface and nucleated atoms above of it. In order to isolate the nucleated atoms effects, the second fluctuation source should be removed. To do that, we compute the averaged PSD from similar locations but on reference wafer, i.e. without material C deposition. The ratio between the PSDs of the wafer under investigation and the reference will be free from bottom layer effects and is called the normalized PSD. The normalized PSDs assessed on samples having various selectivity levels relate that always they have 2 regimes. In low-frequency regime, the normalized PSD is flat while in the high-frequency regime, it has a bump which upward or downward moves according to the number of deposited atoms on the surface. Thus, to quantify nucleations, we have decided to compute the area under the normalized PSD, importantly under the bump which means for the frequency range $[2 \cdot 10^{-3}, 3.5 \cdot 10^{-2}]$ (nm^{-1}).

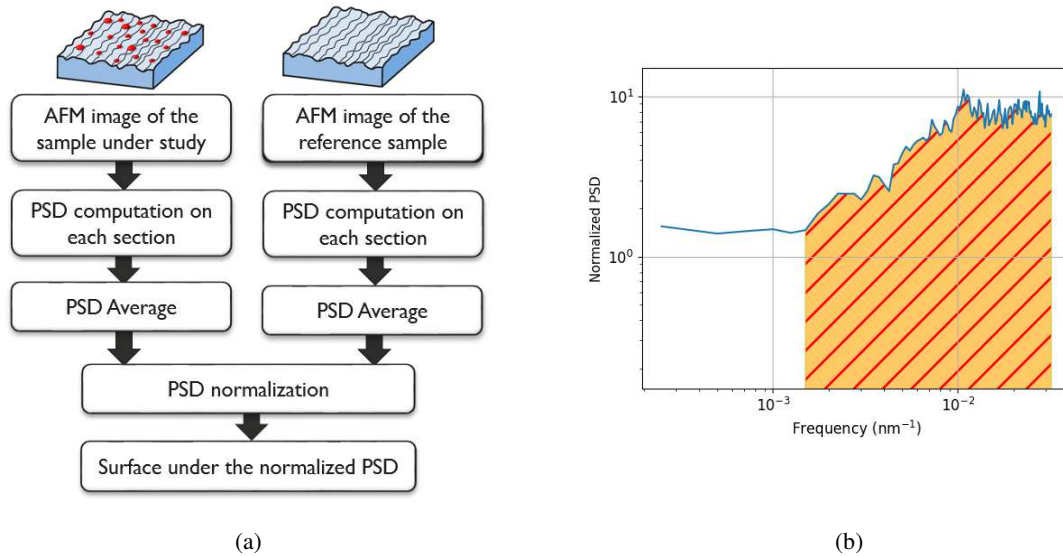


Figure 6: (a) Flowchart of the algorithm allowing the atoms nucleation quantification from AFM images, (b) Nucleation quantification by the computation of the area under the normalized PSD

3. DESIGN OF EXPERIMENT

To validate experimentally the metrology combination proposed in this work, we have used samples composed of SiO₂ lines spaced by trenches filled by W. The ASD process targets to deposit the ZrO₂ selectively above the SiO₂ areas (Figure 7 (a)). The Design of Experiment (DOE) has been carried out by varying the process deposition conditions in order to engender artificially samples with various levels of layer deposition selectivity. Typically, the ZrO₂ deposition conditions vary in the range 30 to 80 as shown in figure 6 (b) and produce distinct deposited configurations of layer thicknesses, lateral overgrowth, and quantity of ZrO₂ nucleated atoms above the non-growth area. We have added to the set of validation wafers, a reference wafer without the ZrO₂ deposition in order to allow PSDs normalization.

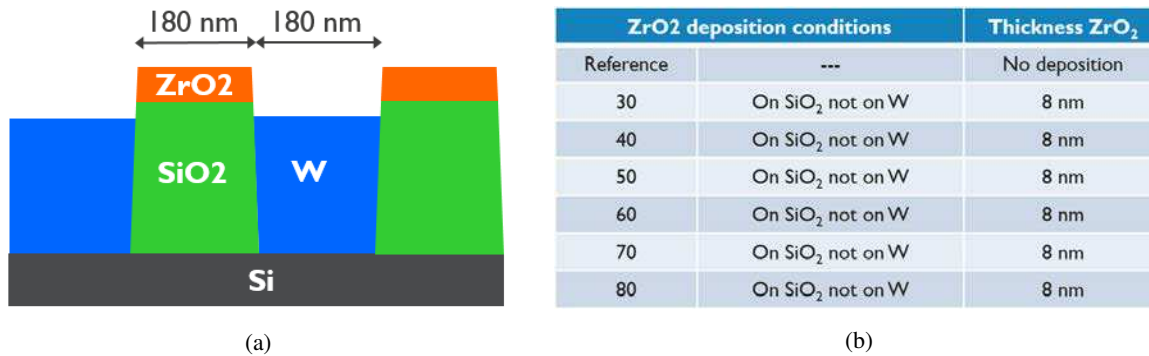


Figure 7: (a) Stack description of the ASD samples, (b) Design of Experiment for the metrology combination validation

4. RESULTS AND DISCUSSION

4.1 Scatterometry results:

In the first section, we show the experimental result obtained by the scatterometry metrology. Figure 8 gives the overview on the thickness of the ZrO₂ layer deposited above the SiO₂ surface (growth area) and displayed as function of the ASD process deposition condition. For each process condition, the data reported corresponds to the measurements across the full wafer surface. Two groups of the ZrO₂ thickness are distinguishable. The first group is formed by the process conditions 30 and 40 which produce thin ZrO₂ layers, with very low thickness included in the range [1, 3] (nm) far from

the target ASD process thickness of 8 nm. These two process conditions are not optimal for the target ASD process. For the remaining process conditions, 50 to 80, the ZrO₂ layer thickness vary in the same range [6, 10] (nm) which is more consistent with the process target. The 4nm thickness dispersion corresponds to the natural dispersion across the wafers surface.

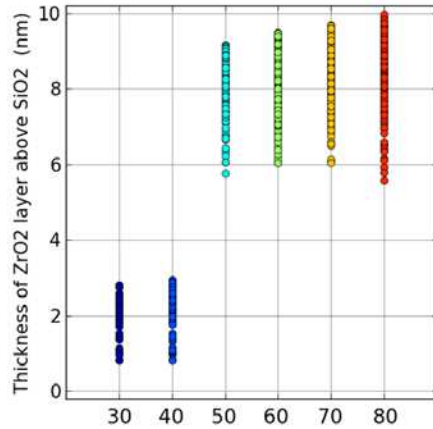


Figure 8: Thickness of the ZrO₂ layer measured above the SiO₂ surface (growth area) as function of the deposition conditions.

The figure 9 shows the full wafer maps of the ZrO₂ layer thickness deposited above the SiO₂ surface for process conditions (a) 30, (b) 40, (c) 50, (d) 60, (e) 70 and (f). 3 different types process signatures are observed for the same thickness where the conditions 30 and 40 have almost radial signature. For conditions 60 and 70, the ZrO₂ thickness is larger in the bottom dies and smaller in the top dies. The wafers processed with conditions 50 and 80 have a reversal of the process signature because the thickness is now larger in the top dies and smaller in the bottom dies.

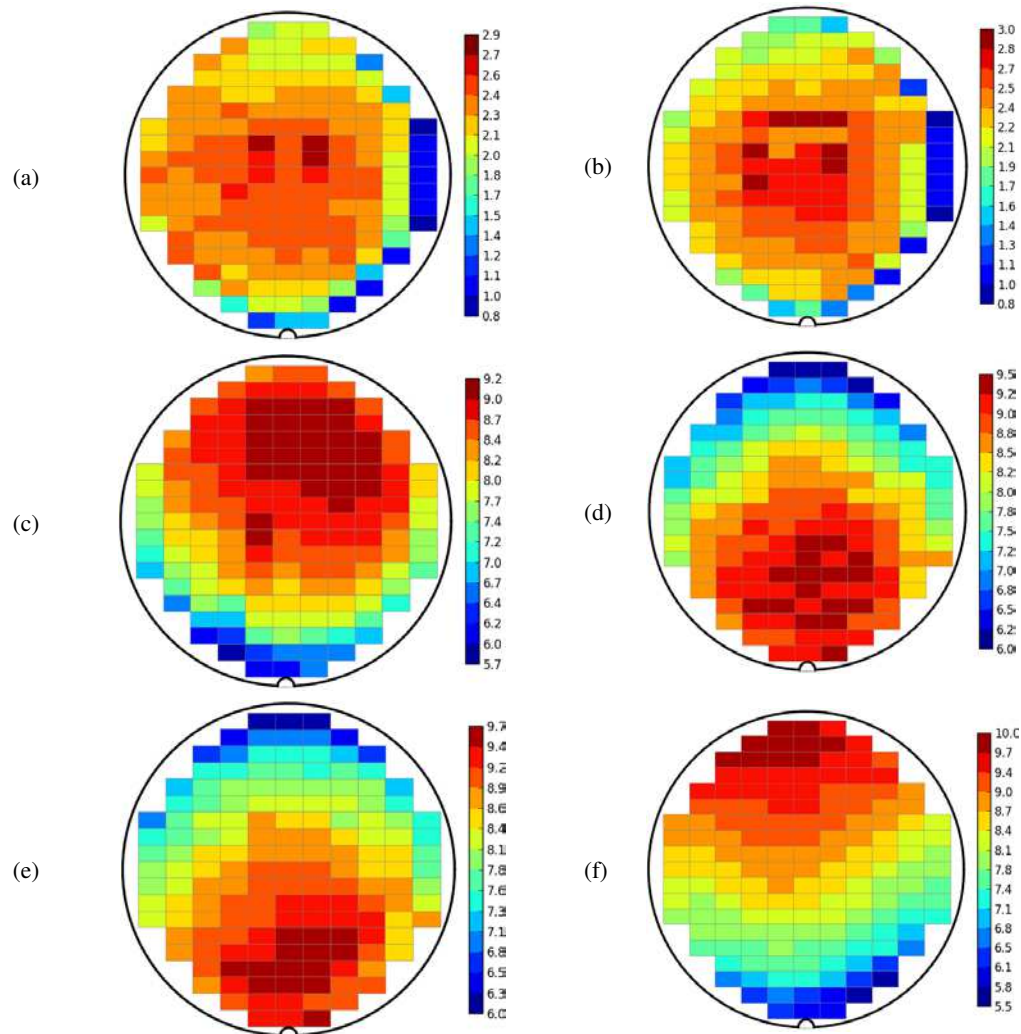


Figure 9: Full wafer maps of the ZrO₂ layer thickness deposited above the SiO₂ surface for process conditions (a) 30, (b) 40, (c) 50, (d) 60, (e) 70 and (f) 80

In the Figure 10 (a), we represent the ZrO₂ layer thickness deposited above the non-growth area (trenches of W). For a good ASD process, no ZrO₂ layer should be deposited on this area. Scatterometry reveals that the process conditions (30 to 70) doesn't induce layer deposition above this surface because the thickness is 0 nm. The process condition 80 is the single configuration in our DOE that causes ZrO₂ layer deposition on the non-growth area. Typically, the ZrO₂ thickness vary between 0 and 7.8 nm. From the wafer map of the Figure 10 (b), we observe that when we exclude the edge dies the ZrO₂ thickness 2 will vary in narrower range which is [4, 7.8] (nm) which confirms that the process selectivity is bad.

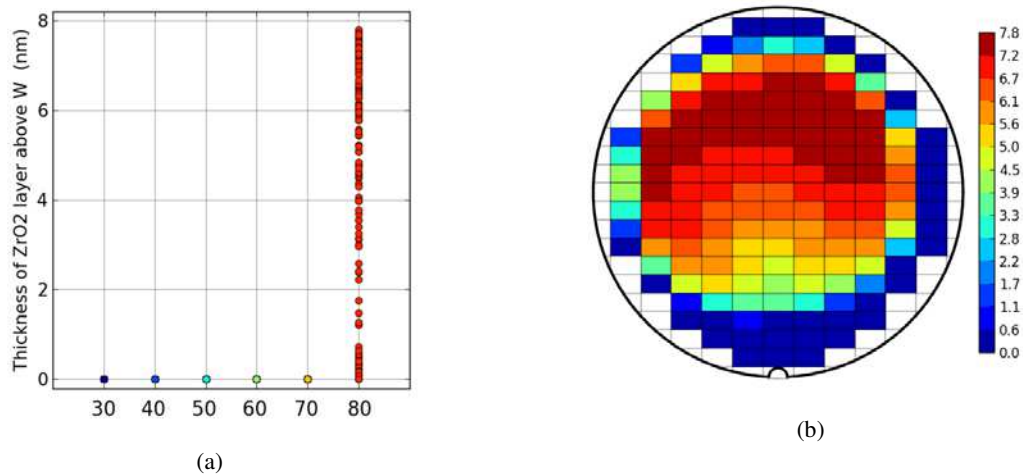


Figure 10: (a) Thickness of the ZrO₂ layer measured above the W surface (non-growth area) as function of the deposition conditions, (b) Wafer map of the thickness of the ZrO₂ layer deposited above the W surface for the wafer processed with the condition 80

The lateral overgrowth is the third parameter reported by scatterometry. It shows the coverage length between the ZrO₂ layer and the adjacent W area when its value is positive. From the Figure 11, we see that the process conditions 30, 40 and 50 don't show any overlap between the ZrO₂ and W. Thus, the ZrO₂ patterns are narrower than the underneath SiO₂ surface. On the second set of samples processed with the conditions 60 to 80, the ZrO₂ area overlap increasingly with the W area due to the layer overgrowth.

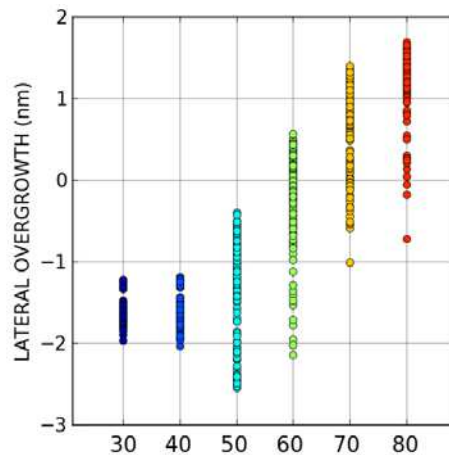


Figure 11: ZrO₂ lateral overgrowth as function of the process deposition condition

To summarize the scatterometry results, the process conditions 30 and 40 are not optimal for the ZrO₂ layer deposition on the ASD growth area. The process condition 80 has a very bad selectivity because of the ZrO₂ layer overlap with W surface. The process conditions 50, 60 and 70 produce similar selectivity performance from point of view of scatterometry, but with various amplitudes of the lateral overgrowth.

4.2 AFM results:

Scatterometry has shown that the process conditions 30 and 40 induce very low ZrO₂ deposition above the growth area. Thereby they are considered as bad conditions for ASD process and were dismissed from the set of investigated wafers with AFM. The AFM has been applied to measure wafers processed with the deposition conditions, 50, 60, 70, 80 and the reference. On each wafer, only 13 dies have been measured across the surface according to the measurement map (Figure 12).

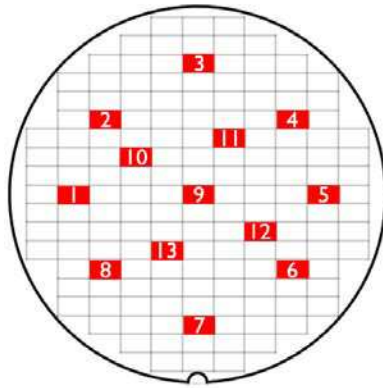


Figure 12: AFM measurement plan

The normalized PSDs averaged by wafer and computed according to the algorithm described in the section 2.2 are displayed on the Figure 13 (a). The calculation has been done on the middle location of the trench for the deposition conditions 50 to 80. The amplitude of the bump's changes from sample to another which is disclosing a diversity of the number of nucleated atoms according to process conditions 50 to 80. As declared before, the area under the normalized PSDs is proportional to the total number of atoms nucleated at that location (Figure 13 (b)). The deposition conditions 50 and 60 show the lowest number of ZrO₂ nucleated atoms, while the condition 80 depicts the largest number of nucleations. The remaining deposition condition (70) is an intermediate configuration but with relatively high number of nucleations compared to the reference.

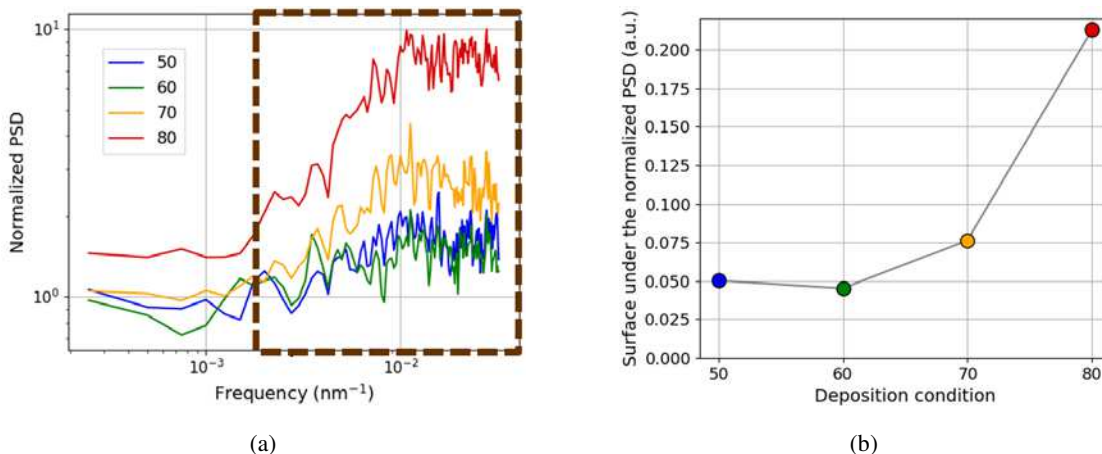


Figure 13: (a) Normalized PSDs computed on the center location of the non-growth area (above W surface) for the ASD samples processed with deposition conditions 50, 60, 70 and 80. (b) Curve of the area under normalized PSD as function of ASD deposition conditions

By extending PSD normalization to the entire width of the trench, we got the full ZrO₂ growth profile along the W area (Figure 14). The first observation shows that the normalized PSD results are stable along W width in term of selectivity performance of the conditions 50 to 80. The condition 60 is best configuration to minimize the ZrO₂ nucleation on the W surface. With the condition 50, a very weak increase of the number of nucleated atoms occurs. The third condition, 70, depicts 50% increase of the nucleation which indicates a degradation of the ASD process selectivity. The last condition, which is 80 is the worst because the very high number of nucleated atoms which is in line with scatterometry results. The averaged profile per wafer also shows that the profile of nucleated atoms along the trench width is uniform (curve almost flat) for the conditions 50, 60 and 70 in contrary to the condition 80 where more atoms are nucleated at the center than close to trench edges.

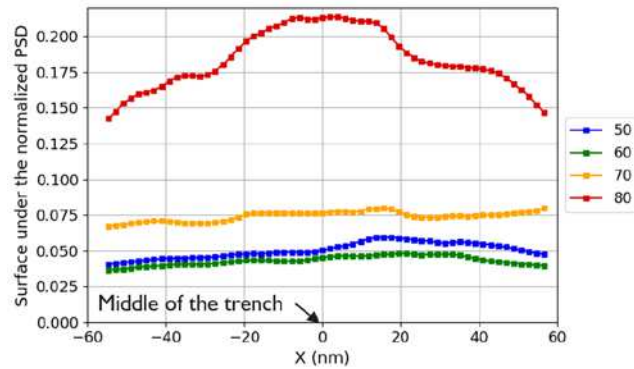


Figure 14: Averaged profile per wafer of the ZrO₂ atoms nucleation across the full W area width

In order to determine the ZrO₂ nucleation mode, we have stacked in the Figure 15 (a) many individual profiles acquired per die of the ZrO₂ atoms nucleation across the full W area width of samples processed with the deposition conditions 50, 60, 70 and 80. We observe that during the initial phase the nucleation of the ZrO₂ is uniform across the non-growth area (figure 15(b)). In the second phase, the center of the trench nucleates slightly more atoms than the edges. And in the third phase, the anisotropic growth at the center of trenches is confirmed and is accelerating.

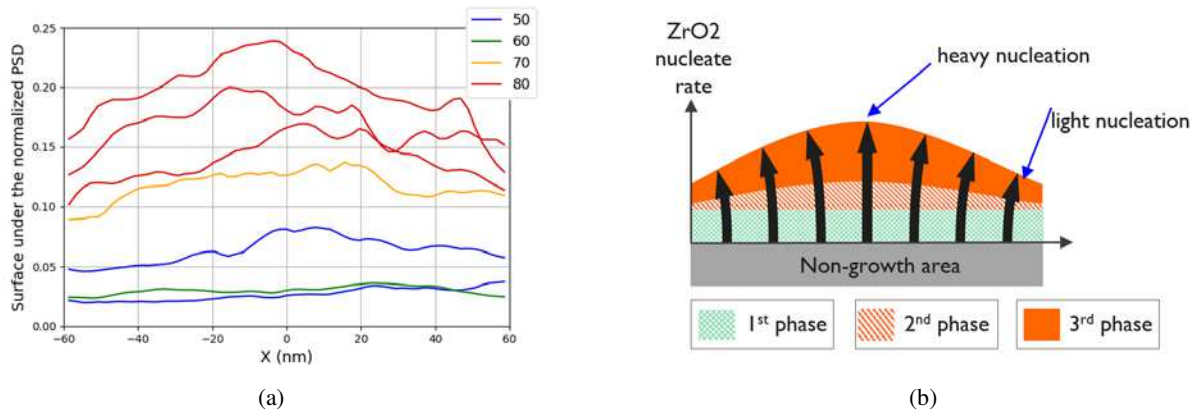


Figure 15: (a) Individual profile per die of the ZrO₂ atoms nucleation across the full W area width of samples processed with the deposition conditions 50, 60, 70 and 80. (b) Representative scheme of the ZrO₂ growth above the W area

4.3 TEM results:

The TEM images have been measured on all ASD samples from wafer Dies (0,0), (0,-6) and (0,+6) in order to check the scatterometry results over wafers surface. On each sample, thin lamellas were picked out on “regular” TEM grids to minimize the measurement disturbance effects. The Figure 16 summarize the TEM results obtained on the sample processed with the deposition conditions (a) 50, (b) 60, (c) 70 and (d) 80. Despite the TEM is very local measurement approach, its results have confirmed the outcomes of scatterometry which is a global metrology. Indeed, the lateral overgrowth is the first geometrical parameter we have compared between the two measurement techniques where they depict the same evolution of the lateral overgrowth according to the ASD deposition conditions. The TEM have shown that for the condition 50, there is no lateral overgrowth while for conditions 60, 70 and 80, it increases continuously. On other hand, the ZrO₂ thickness extracted from TEM images shows a slight increase on its value when the deposition conditions vary from 50 to 80. These results are in good agreement with Scatterometry data shown in the figure 8. The third scatterometry result confirmed by the TEM data is the serious loss in selectivity of the ASD process with condition 80.

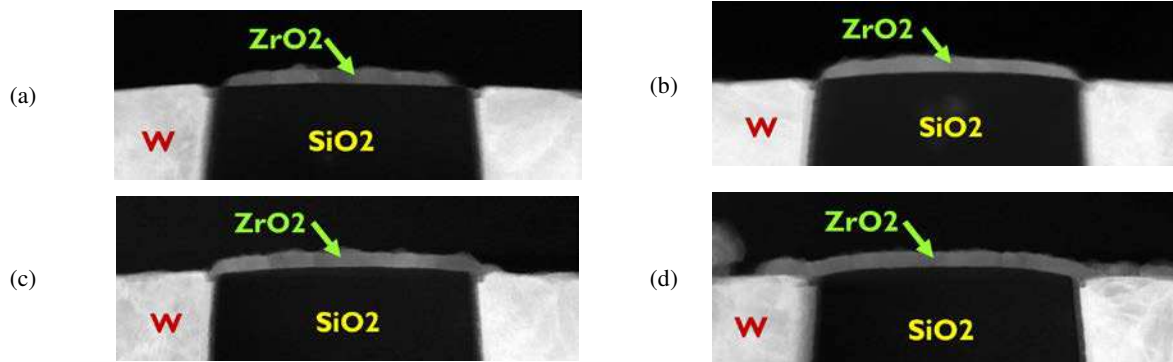


Figure 16: TEM images acquired on ASD samples processed with the deposition conditions (a) 50, (b) 60, (c) 70 and (d) 80.

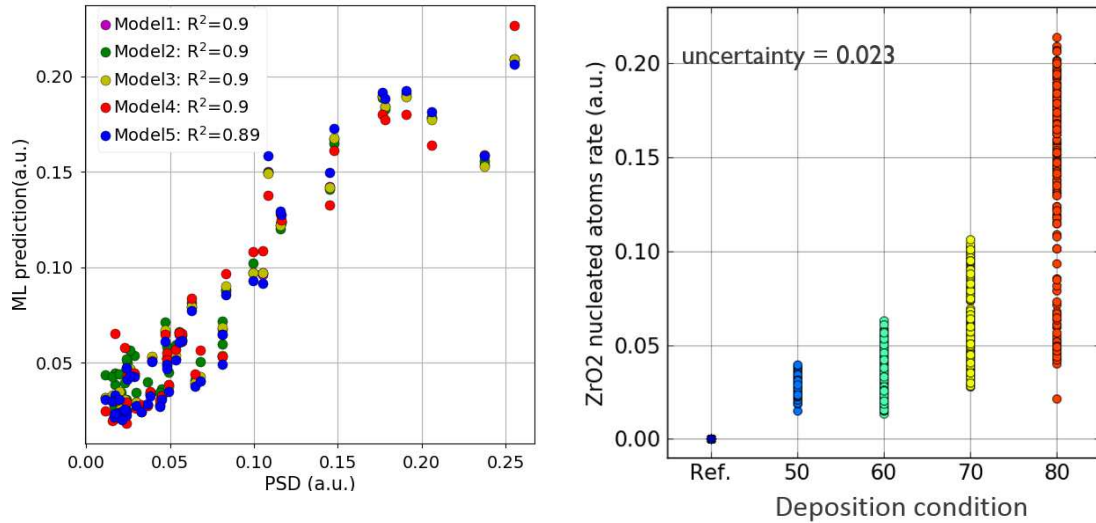
4.4 Machine Learning model:

To extend further the scatterometry metrology capabilities regarding to the quantification of nucleated atoms above the non-growth area, we have used the Nova's machine learning algorithms to train with AFM output, and be able to predict the selectivity property. We have created a mathematical estimator of the quantity of ZrO₂ nucleated atoms by crossing the scatterometry spectra with the PSD data used as a reference. The benefit from the machine learning model is to speed-up the metrology results delivery time because the heavy PSD analysis will be replaced with a very fast predictions. 5 different scenarios (table 1) have been considered concerning the set of data used for the model build to verify its robustness. In the configuration 1 (2), the model has been trained on all PSD data (13 dies/wafer) of the reference wafer and Process Conditions 60, 70, 80 (50,70,80), respectively. For the configurations 3 to 5, the machine learning model has been trained on data coming from reference and the Process conditions 50,60,70, and 80 but by using only 10 dies selected randomly from the 13. For these all configurations, the validation has been done on the total number of data.

Configuration	Training data
1	Reference and Process Conditions 60, 70, 80 (13 dies/wafer)
2	Reference and Process Conditions 50, 70, 80 (13 dies/wafer)
3	Reference and Process Conditions 50, 60, 70, 80 (10 dies/wafer). Samples locations have been chosen randomly (random 1)
4	Reference and Process Conditions 50, 60, 70, 80 (10 dies/wafer). Samples locations have been chosen randomly (random 2)
5	Reference and Process Conditions 50, 60, 70, 80 (10 dies/wafer). Samples locations have been chosen randomly (random 3)

Table 1: Table showing the data used to train the machine learning model for the configurations 1 to 5

The figure 17 (a) shows the correlation chart between the 5 machine learning models predictions and the PSD (reference) data where the worst coefficient of determination is very high, typically $R^2=0.89$. It means that the PSD data are well explained by the machine learning model based on scatterometry spectra and they are predicted with high conformity. The predictions of the model on full dies of reference and conditions 50, 60, 70 and 80 are shown in the figure 17 (b). The maximum error between the 5 models over the wafer dies is 0.023. This means that the sensitivity of the machine learning model is sufficient to distinguish 3 levels of loss in selectivity from our validation samples which are, level 1 for conditions 50 and 60, level 2 obtained with condition 70 and level 3 the process condition 80. Obviously the level 1 is showing the best selectivity while level 3 the worst one. The selectivity performance of conditions 50 and 60 could not be distinguishable with certitude due the lack in metrology sensitivity to such very close behaviours.



(a) (b)

Figure 17: (a) Correlation chart between the machine learning predictor and the reference data (PSD). (b) Prediction of the ZrO₂ nucleated atoms rate above the non-growth area from scatterometry spectra for samples, reference and processed with the deposition conditions 50, 60, 70 and 80.

4.5 Summary of metrology results:

The figure 18 represents the typical stack by process condition as revealed by the combination of the scatterometry and AFM techniques on ASD samples. Whereas the conditions 30 (a) and 40 (b) induce very low growth of the ZrO₂ above the SiO₂ lines compared to the process target, the conditions 70 (e) and 80 (f) engender a bad process selectivity due to the deposition of ZrO₂ on the non-growth areas for these configurations. The thickness of the ZrO₂ on the growth area match well with expectations of the ASD process. The 2 best ASD results are obtained with the conditions 50 (c) and 60 (d). For the condition 60, there is very weak in process selectivity but with lateral overgrowth of the ZrO₂ pattern while for the condition 50, the loss in selectivity slightly increases but without lateral overgrowth.

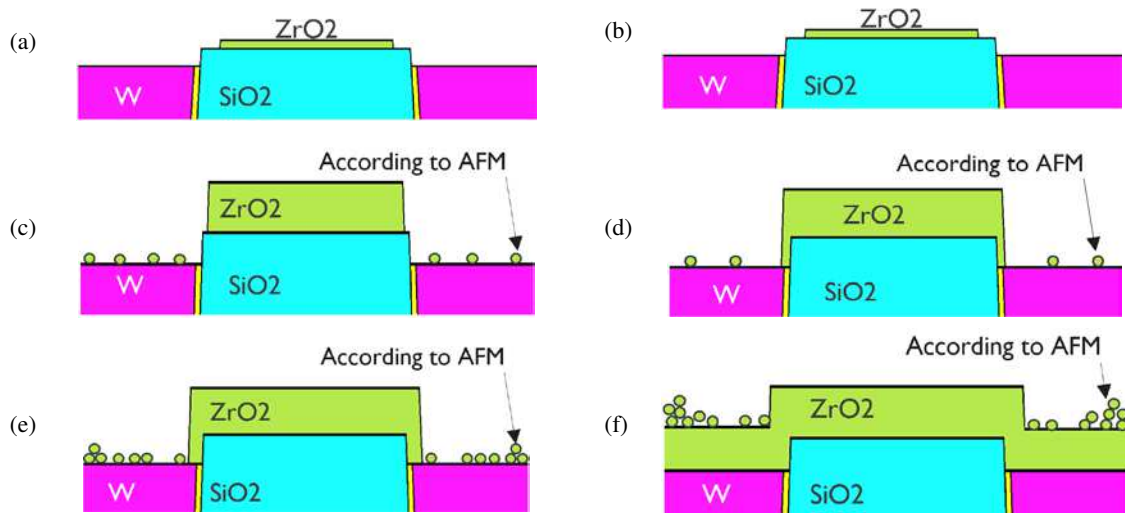


Figure 18: Most typical stack of ASD samples wafer maps of the ZrO₂ layer thickness deposited above the SiO₂ surface for process conditions (a) 30, (b) 40, (c) 50, (d) 60, (e) 70 and (f) 80

5. SUMMARY AND CONCLUSIONS

In this work, a new metrology approach was proposed to characterize the ASD process. The metrology has been built efficiently by the combination of 2 powerful measurement techniques, scatterometry and AFM which were chosen to complement limitations of each other. The scatterometry has measured precisely the geometrical dimension features of the deposited layer, such as the ZrO₂ layer thicknesses above the growth and non-growth surfaces and has identified the sample with poor selectivity. It has measured the lateral overgrowth as well to check the effects of the process on the deposited structure width. To supplement measurements with local samples properties, we have used the AFM and evaluated the atoms nucleation state thanks to an algorithm developed for this work. This technique exploits the topography changes compared to reference as an indicator of atoms nucleation and was able to reveal until to very tiny changes in the process selectivity. Later, the scatterometry machine learning model has been used to mimic the PSD data (obtained from AFM images) and showed good ability to predict until to very weak loss in selectivity of ASD process from scatterometry spectra. This speed-up the analysis of the ASD samples and makes the scatterometry technique powerful for such characterizations.

ACKNOWLEDGMENTS

This project has received funding from the Electronic Component Systems for European Leadership Joint Undertaking under grant agreement No 692522. This Joint Undertaking receives support from the European Union's Horizon 2020 research and innovation program and Netherlands, Belgium, France, Germany, Israel

REFERENCES

- 1: B. N. J. Persson, O. Albohr, U. Tartaglino, A. I. Volokitin and E. Tosatti, "On the nature of surface roughness with application to contact mechanics, sealing, rubber friction and adhesion", *Journal of Physics: Condensed Matter*, 17(1), (2004).
- 2: A. Vaid, B. B. Yan, Y. T. Jiang, M. Kelling, C. Hartig, J. Allgair, P. Ebersbach, M. Sendelbach, N. Rana, A. Katnani, E. Mclellan, C. Archie, C. Bozdog, H. Kim, M. Sandler, S. Ng, B. Sherman, B. Brill, I. Turovets, R. Urensky, "A Holistic Metrology Approach: Hybrid Metrology Utilizing Scatterometry, CD-AFM and CD-SEM", *Proc. of SPIE Vol. 7971, 797103* (2011)
- 3: S. Levi, I. Schwarzband, Y. Weinberg, R. Cornell, O. Adan, G. M. Cohen, L. Gignac, S. Bangsaruntip, S. Hand, J. Osborne, A. Feinstein, "CDSEM AFM Hybrid metrology for the characterization of Gate-All-Around Silicon Nano Wires", *Proc. of SPIE Vol. 9050 905008-2* (2014)
- 4: N. Rana, C. Archie, "Hybrid reference metrology exploiting patterning simulation", *Proc. of SPIE Vol. 7638 76380W-1* (2010)
- 5: J. Foucher, N. Griesbach Schuch Figueiro, J. Rouxel, R. Thérèse, "Hybrid metrology for critical dimension based on scanning methods for IC manufacturing", *Proc. of SPIE Vol. 8378 83780F-1* (2012)
- 6: G. N. Parsons, "ALD Nucleation and Area-Selective Deposition", iitc conference, http://www.iitc-conference.org/uploads/2/4/1/1/24114461/lecture_4_greg_parsons.pdf
- 7: A. Marnett, M. J. M. Merckx, B. Karasulu, F. Roozeboom, W. (Erwin) M. M. Kessels, and A. J. M. Mackus, "Area Selective Atomic Layer Deposition of SiO₂ Using Acetylacetone as a Chemoselective Inhibitor in an ABC-Type Cycle", *ACS Nano* 2017, 11, 9303–9311
- 8: R. Vallat, R. Gassilloud, B. Eychenne, and Ch. Vallée, "Selective deposition of Ta₂O₅ by adding plasma etching super-cycles in plasma enhanced atomic layer deposition steps", *J. Vac. Sci. Technol. A* 35(1), 01B104-1 (2017)
- 9: R. L. Puurunen, W. Vandervorst, W. F. A. Besling, O. Richard, H. Bender, T. Conard, C. Zhao, A. Delabie, M. Caymax, S. De Gendt, M. Heyns, M. M. Viitanen, M. de Ridder, H. H. Brongersma, Y. Tamminga, T. Dao, T. de Win, M. Verheijen, M. Kaiser, and M. Tuominen, "Island growth in the atomic layer deposition of zirconium oxide and aluminum oxide on hydrogen-terminated silicon: Growth mode modeling and transmission electron microscopy", *J. Appl. Phys.*, Vol. 96, No. 9, 1 November 2004

- 10: G. F. Lorusso, T. Sutani, V. Rutigliani, F. v. Roey, A. Moussa, A.-L. Charley, C. Mack, P. Naulleau, C. Perera, V. Constantoudis, M. Ikota, T. Ishimoto, S. Koshihara, "Need for LWR metrology standardization: the imec roughness protocol", *J. Micro/Nanolith. MEMS MOEMS* 17(4), 041009 (Oct–Dec 2018)
- 11: V. Rutigliani, G. F. Lorusso, D. D. Simone, F. Lazzarino, G. Papavieros, E. Gogolides, V. Constantoudis, C. A. Mack, "Setting up a proper power spectral density and autocorrelation analysis for material and process characterization", *J. Micro/Nanolith. MEMS MOEMS* 17(4), 041016 (Oct–Dec 2018)